JEEEIT TRANSACTIONS, Vol.03,No.01,July 2026

EEG-Based Brain–Computer Interface for Intelligent Wheelchair Control: A Machine Learning Approach

Hend A. Eissa[1], Abdulrauf A. Aqreerah[2], Hasan N. Ali[1]

[1]Computer Engineering Department, College of Electronic Technology, Tripoli, Libya
[2] Control Engineering Department, College of Electronic Technology, Bani Walid, Libya

Corresponding author: Author one (namarek2010@gmail.com / hasan.naji2010@gmail.com).

ABSTRACT Electroencephalography (EEG)-based motor imagery brain–computer interfaces (BCIs) offer a noninvasive means of control for individuals with severe motor impairments, but their translation into physically actuated systems remains challenged by the inherent uncertainty of EEG decoding. This thesis presents the design, implementation, and evaluation of an EEG-based motor imagery BCI for wheelchair control, integrating a Filter Bank Common Spatial Pattern (FBCSP) feature extraction pipeline with a comparative evaluation of three classifiers, Support Vector Machine (SVM), k-Nearest Neighbors (KNN), and Linear Discriminant Analysis (LDA), on the BCI Competition IV Dataset 2a under a subject-dependent paradigm. Using five-fold stratified cross-validation, SVM achieved the highest mean accuracy (90.7 ± 2.6%) and Cohen's Kappa (0.876 ± 0.035), and was subsequently evaluated on an independent, unseen dataset via a replay based Hardware-in-the-Loop (HIL) methodology, achieving 85.9% accuracy. A confidence-based command validation stage further improved reliability, raising accuracy among accepted predictions to 97.6% at 60.7% coverage. The classifier output was interfaced with a physical differential-drive wheelchair prototype governed by an encoder-based closed-loop steering control scheme. A multi-tiered safety strategy, comprising confidence gating, self-terminating steering, transition braking, communication timeout supervision, and a hardware emergency cutoff, was incorporated to constrain the consequences of residual classification uncertainty. These results demonstrate that careful integration of classification, command validation, and embedded safety design can yield a robust and practical EEG-based wheelchair control framework, despite the imperfect reliability of motor imagery decoding.

KEYWORDS Brain–Computer Interface, EEG, Motor Imagery, Wheelchair Control, Filter-Bank Common Spatial Patterns, Support Vector Machine, Linear Discriminant Analysis, and k-Nearest Neighbors

I. INTRODUCTION

Brain–Computer Interfaces (BCIs) establish a direct communication pathway between the brain and external devices by translating neurophysiological activity into machine-interpretable commands [1]. This technology is particularly important for individuals with severe motor impairments, such as spinal cord injuries or amyotrophic lateral sclerosis (ALS), who may be unable to operate conventional assistive systems [2]. Among non-invasive BCI modalities, electroencephalography (EEG) is widely used due to its portability, low cost, and high temporal resolution. However, EEG signals are characterized by low signal-to-noise ratio and are easily affected by physiological and environmental artifacts, making reliable decoding a significant challenge.

Motor imagery (MI)-based BCIs represent one of the most promising approaches for EEG-based control applications. In MI tasks, users imagine specific limb movements without producing actual muscle activity, generating characteristic modulations in sensorimotor rhythms, particularly within the μ and β frequency bands [2]. These patterns can be exploited to generate control commands for assistive devices such as robotic wheelchairs. Nevertheless, accurate and reliable classification of MI signals remains difficult because of EEG variability, noise, and overlap between mental tasks [1].

In this work, we propose a non-invasive EEGbased BCI framework for intelligent wheelchair control using a four-class motor imagery paradigm. The framework employs Filter-Bank Common Spatial Patterns (FBCSP) for spatial spectral feature extraction, followed by a comparative evaluation of three machine learning classifiers, namely Support Vector Machine (SVM), k-Nearest Neighbors (KNN), and Linear Discriminant Analysis (LDA). The classifier achieving the best cross-validation performance was subsequently selected for integration with a microcontroller-based differential drive wheelchair

Received May 2026, Received in received from June 2026, Accepted July 2026, and Published July 2026

prototype. To assess the practical behavior of the selected classification approach, the complete control framework was further evaluated using a replay-based Hardware-in-the-Loop (HIL) experiment with unseen dataset., incorporating confidence-based command validation.

The remainder of this paper is organized as follows. Section II presents the proposed methodology, including EEG preprocessing, FBCSP feature extraction, the evaluated classification methods, hardware integration, wheelchair motion control, and safety mechanisms. Section III presents the comparative classifier evaluation and the subsequent replay-based HIL assessment using the unseen dataset.

II. METHODOLOGY

A. Preprocessing

To develop the proposed BCI system, we utilized the publicly available *BCI Competition IV Dataset 2a*, which includes EEG recordings from subjects performing four motor imagery tasks: left-hand, right-hand, both-feet, and tongue imagery [3].

The signals were recorded using 22 Ag/AgCl electrodes placed according to the international 10– 20 system, primarily covering the sensorimotor cortex, and were sampled at 250 Hz. In addition, three monopolar EOG channels were recorded for artifact detection purposes. Only the 22 EEG channels were retained for analysis, while the EOG channels were excluded from the classification pipeline [4].

In this work, only the EEG recordings of a single subject from the BCI Competition IV Dataset 2a were considered. Therefore, the study follows a subject-dependent classification paradigm, where all preprocessing, feature extraction, model training, and evaluation stages were conducted using data from the same subject.

A four-class MI paradigm consisting of left-hand, right-hand, feet, and tongue imagery was adopted. These motor imagery classes were subsequently mapped to wheelchair control commands, enabling lateral steering, forward motion, and an auxiliary command such as stopping. Employing an existing benchmark dataset allows the algorithmic components of the system to be designed and tuned offline under controlled and reproducible conditions.

Prior to feature extraction, the EEG data underwent a sequence of preprocessing operations aimed at improving signal quality and suppressing non-cortical artifacts. Each continuous recording was first segmented into individual motor imagery epochs using a 0.5–3.5 s window relative to cue onset, yielding segments of 750 samples per trial. Trials flagged as artifact-contaminated in the dataset annotations were then excluded from further analysis. Common Average Referencing (CAR) was subsequently applied to the artifact-free epochs to suppress spatially correlated activity shared across channels and to improve the reliability of the spatial covariance estimates used downstream by CSP [5] [6].

Finally, a fourth-order Butterworth band-pass filter (4–30 Hz) was applied to the CAR-referenced signals as a broad pre-filtering stage prior to FBCSP decomposition, reducing low-frequency drifts and high-frequency noise while preserving the frequency components relevant to motor imagery processing [7]. The resulting artifact-free, CAR referenced, band-limited signals were then forwarded to the FBCSP feature extraction stage.

B. Feature Extraction using FBCSP

To capture the discriminative spatial–spectral patterns of motor imagery (MI) EEG signals, a Filter Bank Common Spatial Patterns (FBCSP) framework was employed. FBCSP extends the conventional CSP method by decomposing EEG signals into multiple frequency sub-bands, allowing the model to exploit subject-specific spectral characteristics of MI-related activity, particularly within the μ and β rhythms [8], [9].

1) Filter Bank Decomposition: Following preprocessing, each EEG trial was decomposed into multiple frequency bands using a bank of fourth order Butterworth band-pass filters. The filter bank comprised 12 overlapping frequency bands covering the sensorimotor μ and β rhythms, which are known to contain the most discriminative information for motor imagery classification. Specifically, ten narrow sub-bands spanning 8–30 Hz were defined with a bandwidth of 4 Hz and a step size of 2 Hz (8–12, 10–14, ..., 26–30 Hz), while two wider bands corresponding to the complete physiological μ (8–13 Hz) and β (13–30 Hz) rhythms were additionally included to preserve rhythm-level oscillatory information. This multi-band decomposition enables the extraction of complementary spatial spectral information distributed across different frequency ranges, thereby improving classification performance compared with conventional single band CSP approaches [8], [10].

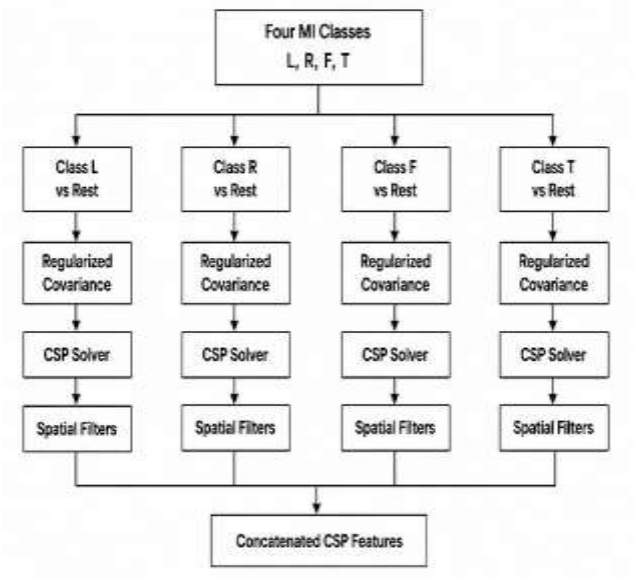

FIGURE 1. Workflow of One-vs-Rest Common Spatial Pattern.

2) *One-vs-Rest CSP with Regularization:* Since CSP is inherently formulated as a two-class spatial filtering method for two class discrimination through a generalized eigenvalue problem that maximizes variance for one class relative to another, a One-vs-Rest (OVR) strategy was adopted to extend it to the four class setting. In this approach, each class is treated as the target class, while the remaining classes are combined to form a competing class. This results in a series of binary CSP problems, each learning spatial filters by maximizing the variance of the target class relative to the aggregated covariance of the remaining classes [11], [12]. The complete OVR-CSP procedure adopted in this work is illustrated in Figure 1.

Let $\mathbf{X} \in \mathrm{R}^{C\times T}$ denote an EEG trial with C channels and T time samples. The sample covariance matrix was first regularized to improve numerical stability

$$\mathcal{R}_{\mathrm{REG}} = XX^T + \varepsilon I \tag{1}$$

Where $\varepsilon = 10^6$, and subsequently trace normalized to remove the influence of overall signal power,

$$\mathcal{R} = \frac{\mathcal{R}_{\mathrm{REG}}}{\mathrm{TRACE}(\mathcal{R}_{\mathrm{REG}})} \tag{2}$$

For each class, CSP filters were obtained by solving the generalized eigenvalue problem

$$\mathcal{R}_{\mathrm{CLASS}} w = \eta(\mathcal{R}_{\mathrm{CLASS}} + \mathcal{R}_{\mathrm{REST}})w \tag{3}$$

where η denotes the generalized eigenvalue. The resulting spatial filters maximize class-specific variance differences. For each class, the most discriminative filters (corresponding to the largest and smallest eigenvalues) were retained [11].

3**) Feature Construction**: The EEG signals were projected onto the CSP filters, and log-variance features were extracted:

$$f_i = \log\left(\frac{\mathrm{var}(z_i)}{\sum_j \mathrm{var}(z_j)}\right) \tag{4}$$

where z_i is the i-th spatially filtered signal. These features are known to follow approximately Gaussian distributions, making them suitable for linear and kernel-based classifiers [9].

Features from all frequency bands and classes were concatenated to form the final feature vector.

4) Feature Selection: Due to the high dimensionality of the features generated by the FBCSP framework (384 features across 12 sub-bands), feature selection was performed using Mutual Information (MI) to rank the extracted features according to their relevance to the target classes. The number of retained features was set to K = 80, chosen to keep the feature dimensionality well below the number of available training trials and thereby mitigate the risk of overfitting associated with high-dimensional, limited-sample classification problems, while still retaining sufficient discriminative information across multiple frequency sub-bands. This approach has been shown to enhance FBCSP-based classification performance by focusing on the most informative features [13], [14].

Fig 2 summarizes the overall FBCSP-based feature extraction and classification pipeline employed in this study.

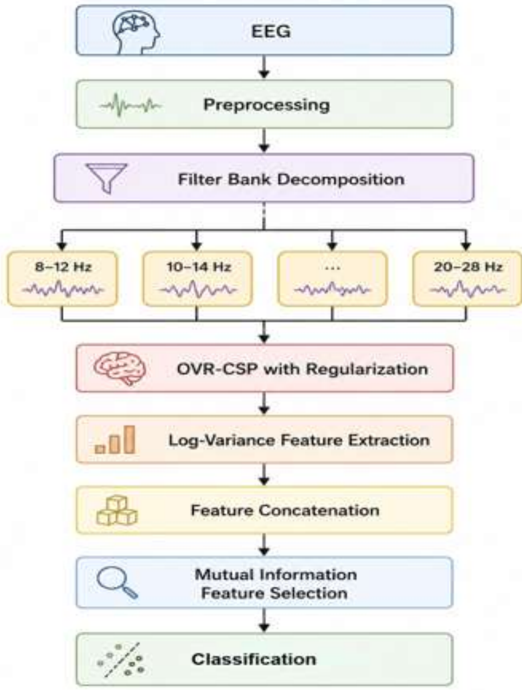

FIGURE 2. Overview of the proposed FBCSP-based feature extraction and classification pipeline.

C. *Classification Methods*

1) **Support Vector Machine:** Support Vector Machine **(SVM)** is a supervised learning algorithm widely employed for **EEG** signal classification due to its strong generalization capability and effectiveness in high-dimensional feature spaces [15], [16]. Given training samples (x_i, y_i) with $x_i \in \mathrm{R}^d$ and $y_i \in \{-1, +1\}$, SVM seeks a separating hyperplane that maximizes the margin between classes [17]. To accommodate the overlapping class distributions typical of **EEG**-derived features, a soft-margin formulation was adopted, introducing a slack variable $\zeta_i \geq 0$ per sample and solving.

$$W^T X + b = 0 \tag{5}$$

$$\min_{\mathbf{w},b,\xi} \quad \frac{1}{2}\|\mathbf{w}\|^2 + C\sum_{i=1}^{N} \xi_i, \tag{6}$$

subject to $y_i(\mathbf{w}^{\mathrm{T}}\mathbf{x}_i + b) \geq 1 - \xi_i, \ \xi_i \geq 0,$
where C controls the trade-off between margin width and training error [17]. The dual formulation expresses the decision function in terms of sample dot products,

Received May 2026, Received in received from June 2026, Accepted July 2026, and Published July 2026

$$f(\mathbf{x}) = \sum_{i=1}^{N} \alpha_i y_i \left(\mathbf{x}_i^{\mathrm{T}} \mathbf{x}\right) + b, \tag{7}$$

allowing the dot product to be replaced by a kernel function to construct nonlinear decision boundaries. A Gaussian (RBF) kernel was used,

$$K(\mathbf{x}_i, \mathbf{x}_j) = \exp\left(-\gamma \|\mathbf{x}_i - \mathbf{x}_j\|^2\right) \tag{8}$$

with $\gamma > 0$ controlling the width of the Gaussian and hence how far the influence of a training sample extends in the feature space. The RBF kernel was selected as it provided slightly better accuracy than a linear kernel in preliminary tests, consistent with the expected non-linear separability of some class combinations in the FBCSP feature space [15], [18]. The four-class motor imagery problem was addressed using the One-vs-One (OvO) decomposition strategy, training a separate binary classifier for every pair of classes ($\binom{4}{2} = 6$ classifiers in total). During prediction, each pairwise classifier casts a vote, and the class receiving the majority of votes is selected as the final output [19]. Multiclass SVM strategies have been widely investigated for motor imagery EEG classification, including evaluations on BCI Competition datasets [10].

The hyperparameters C and γ were optimized via grid search with 5-fold cross-validation on the training set with feature extraction, feature selection, and standardization refit independently within each fold to prevent information leakage [20].

2) **k-Nearest Neighbors:** k-Nearest Neighbors **(KNN)** is a non-parametric classification method that makes no assumption about the underlying distribution of the feature space and has been investigated as a conventional classifier for motor imagery **EEG** classification problems [21]. A test sample is classified based on the labels of its closest training samples in the standardized 80-dimensional **FBCSP** feature space, measured using the Euclidean distance,

$$d(\mathbf{x}, \mathbf{x}_i) = \|\mathbf{x} - \mathbf{x}_i\|_2 = \sqrt{\sum_{j=1}^{d} (x_j - x_{i,j})^2}. \tag{9}$$

The k training samples with the smallest distance to x form its neighborhood $\aleph_K(X)$. A distance weighted voting scheme was adopted, in which each neighbor's contribution is weighted by the inverse of its distance to the query sample,

$$w_i = \frac{1}{d(\mathbf{x}, \mathbf{x}_i) + \epsilon}, \tag{10}$$

where ϵ is a small constant preventing division by zero. The predicted class label is given by the class that maximizes the sum of neighbor weights,

$$\hat{y} = \arg\max_k \sum_{i \in \mathcal{N}_k(\mathbf{x})} w_i \cdot \mathbb{I}(y_i = k), \tag{11}$$

where $\mathbb{I}(\cdot)$ is the indicator function. Distance weighting was adopted so that nearby, more relevant training samples dominate the classification decision over more distant ones within the neighborhood
[22].

In the proposed implementation, k = 5 neighbors were used with the Euclidean distance metric, consistent with the standardized FBCSP feature vectors following z-score normalization. As with the other classifiers, feature extraction, feature selection, and standardization were refit independently within each cross-validation fold to prevent information leakage.

3) Linear Discriminant Analysis: Linear Discriminant Analysis (LDA) was employed as a linear classifier based on Fisher's discriminant criterion [22]. LDA has been widely investigated as a baseline classifier for motor-imagery EEG classification due to its low computational complexity and compatibility with CSP/FBCSP-derived feature representations [18], [23].

LDA assumes that the feature vectors of each class follow a multivariate Gaussian distribution with class-specific means μk but a common covariance matrix Σ, estimated by aggregating the within class covariance across all classes [22].

$$p(\mathbf{x} \mid y = k) = \mathcal{N}(\mathbf{x}; \boldsymbol{\mu}_k, \boldsymbol{\Sigma}). \tag{12}$$

Under this assumption, the class posterior probabilities reduce to a set of linear discriminant functions,

$$\delta_k(\mathbf{x}) = \mathbf{x}^{\mathrm{T}} \boldsymbol{\Sigma}^{-1} \boldsymbol{\mu}_k - \frac{1}{2} \boldsymbol{\mu}_k^{\mathrm{T}} \boldsymbol{\Sigma}^{-1} \boldsymbol{\mu}_k + \log \pi_k, \tag{13}$$

where πk denotes the prior probability of class k, estimated from the class frequencies in the training data. A sample x is assigned to the class k that maximizes $\delta_K(x)$, and since $\delta_K(x)$ is linear in x, the resulting decision boundaries between classes are hyperplanes.

The pooled within-class covariance matrix was estimated via singular value decomposition (SVD), which remains numerically stable even when the feature covariance matrix approaches singularity, without requiring an additional shrinkage hyperparameter. The discriminant functions $\delta_K(x)$ were computed directly for all four motor imagery classes simultaneously, with the class yielding the highest discriminant score selected as the predicted label [22]. The SVD solver was applied directly to the standardized 80-dimensional FBCSP feature vectors within each cross-validation fold.

D. Hardware Integration and Wheelchair Control Interface

The final component of the proposed system is the interface between the EEG classification framework running on a host computer and the motorized wheelchair platform.

1) System Architecture Overview: The overall architecture of the proposed EEG-based wheelchair control system is illustrated in Fig. 3. The system follows a layered design comprising three stages: (1) EEG processing and classification on the host PC, (2) software-level command validation, and (3) embedded motion execution on a microcontroller-based platform. Among the classifiers described in Section II, the classifier achieving the highest cross-validated performance reported in Section III was subsequently selected to drive the prototype wheelchair. Hardware validation of the classifier was carried out using a replay-based hardware-in-the-loop (HIL) approach, described in Section II-D4.

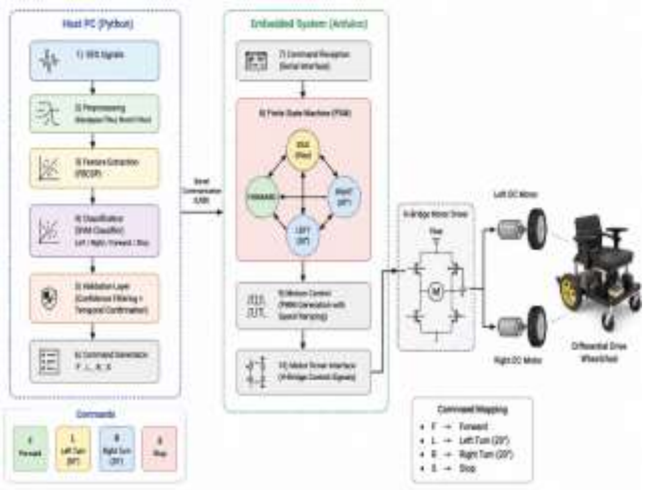

FIGURE 3. Overall architecture of the proposed EEG based wheelchair control system.

2**) Wheelchair Prototype and Actuation Hardware**: For experimental validation, a small-scale differential-drive wheelchair prototype was constructed, consisting of two independently driven DC gear motors mounted on a wheelbase of L = 0.14625 m, controlled through an L298N dual Hbridge motor driver. Each drive wheel (diameter D = 0.065 m) was fitted with a quadrature incremental rotary encoder to provide direct feedback on wheel rotation for closed-loop steering control, as described in Section II-E. The prototype was powered by a 9 V battery pack. A caster wheel was used at the rear of the chassis to provide passive support and maintain balance during turning maneuvers. An Arduino Uno microcontroller was used as the embedded actuation controller, interfacing with the motor driver through digital PWM output pins for speed control and digital output pins for direction control, and with the two-channel (A/B) quadrature outputs of the wheel encoders through interrupt capable digital input pins for pulse counting and direction detection.

3) **Communication Protocol**: High-level motion commands generated by the EEG processing software (implemented in Python) are transmitted from the host PC to the Arduino through a serial (USB) communication interface operating at a baud rate of 9600 bps. The communication protocol uses single character symbolic commands, where right-hand imagery results in transmission of the command R, initiating a right turn, while left-hand imagery generates the command L for left steering. Foot imagery corresponds to the command F for forward motion, whereas tongue imagery produces the command S, which halts wheelchair motion.

4) **Replay-Based Hardware-in-the-Loop (HIL):** A replay-based Hardware-in-the-Loop (HIL) methodology was employed to evaluate the proposed wheelchair control framework. Previously unseen EEG trials from the same subject were sequentially replayed to the trained classifier, while the resulting predictions were subsequently forwarded to the embedded control system for motion execution. The trained classifier processes replayed unseen trials at fixed intervals of 1s, emulating the cadence of a continuously operating system. For each replayed trial, the classifier produces a probability score for each of the four motor-imagery classes. Decision confidence is defined as the maximum probability among these four scores. A confidence-based validation stage is then applied prior to command execution. Specifically, only predictions with a confidence value greater than or equal to a defined confidence threshold are accepted and transmitted to the Arduino controller for execution, while predictions below this threshold are rejected to prevent potentially unreliable wheelchair commands. Because all replayed EEG trials are drawn from an unseen dataset excluded from both model training and cross-validation, the HIL procedure evaluates the complete decision-making pipeline under previously unseen EEG data. This methodology enables functional verification of command generation and execution while avoiding optimistic performance estimates associated with evaluation on the training data.

E. Embedded Motion Control and Command Execution Strategy

The embedded control subsystem is responsible for stable and safe execution of validated motion commands received from the EEG processing framework. Since direct execution of incoming commands may result in abrupt or unstable wheelchair behavior, a supervisory motion-control strategy is employed at the embedded level.

1**) Finite State Machine Design**: At the embedded level, wheelchair motion is governed by a deterministic finite state machine (FSM) comprising four predefined motion states: IDLE/STOP, FORWARD, LEFT, and RIGHT. The FSM provides a structured control framework for governing motion-state transitions, thereby improving operational safety and motion stability. In the IDLE/STOP state both drive wheels are stationary; in FORWARD, both wheels rotate together at equal velocity; and in the LEFT and RIGHT states, the wheels rotate at equal magnitude but opposite direction, producing a rotational maneuver about the midpoint of the drive axle, as detailed in Section II-E.

Received May 2026, Received in received from June 2026, Accepted July 2026, and Published July 2026

The LEFT and RIGHT states are implemented as discrete incremental steering actions rather than continuous rotational commands. Each valid L or R command initiates a fixed angular rotation of approximately 20◦, after which the controller terminates the turning action and returns to the IDLE state. Each validated command received through the serial interface triggers a transition to the corresponding motion state, as illustrated in Fig. 4.

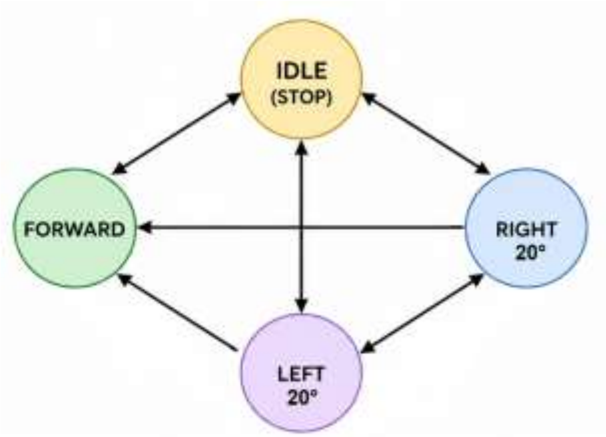

FIGURE 4. **Finite state machine governing embedded motion execution.**

2) Encoder-Based Incremental Steering: Table I defines the wheel-velocity command associated with each motion state, following the differential-drive configuration. In the IDLE/STOP state both wheels are stationary; in FORWARD, both wheels rotate together at equal velocity V ; and in the LEFT and RIGHT states, the wheels rotate at equal magnitude but opposite direction, producing a rotational maneuver about the midpoint of the drive axle. In both steering states, the general relationship $V_r = -V_l$ holds.

TABLE I. WHEEL-VELOCITY COMMANDS PER MOTION STATE

State	V_l	V_r
IDLE/STOP	0	0
FORWARD	V	V
LEFT	$-V$	V
RIGHT	V	$-V$

Incremental steering is implemented using closed-loop feedback from quadrature rotary encoders mounted on the drive wheels, a standard approach for achieving accurate motion control in differential-drive mobile robots [24]. The controller continuously estimates the wheelchair heading from encoder measurements and terminates the turning maneuver when the target angular displacement of approximately 20◦ is reached. The steering increment was selected to provide a practical trade-off between steering precision and command efficiency. Smaller steering increments require a larger number of EEG commands to achieve significant heading changes, increasing response time and user workload, whereas larger increments reduce maneuvering precision. An increment of approximately 20◦ was found to provide an effective balance for the proposed wheelchair prototype. Each encoder disc provides 20 slots per revolution; using quadrature decoding on both channels (A and B) and counting both signal edges yields an effective resolution of N_{ppr} = 80 counts per revolution. The linear distance traveled by a wheel is computed from the accumulated pulse count n as:

$$\Delta s = \frac{\pi D}{N_{ppr}}, \qquad s = n \cdot \Delta s, \tag{14}$$

where D = 0.065 m is the wheel diameter, giving $\Delta s \approx 2.5525$ mm per encoder count.

Since both wheels accumulate the same pulse count n while rotating in opposite directions during a turn, the resulting angular displacement of the wheelchair is:

$$\theta = \frac{s_r - s_l}{L} = \frac{2n\Delta s}{L} \tag{15}$$

where L is the wheelbase of the prototype. The wheelbase was precisely calculated so that the target rotation of 20◦ corresponds to an exact integer number of encoder pulses. Solving for L with θ = 20◦ (0.349066 rad) and n = 10 pulses gives the following.

$$L = \frac{2n\Delta s}{\theta} = \frac{2(10)(0.0025525)}{0.349066} \approx 0.14625 \text{ m.} \tag{16}$$

Consequently, the wheelbase of the prototype was specifically set to L = 0.14625 m (14.625 cm), so that the 20◦ turning maneuver is completed after exactly 10 encoder pulses on each wheel, with no residual fractional pulse count at the target angle. It should be noted that this exact alignment is specifically valid for the 20◦ steering increment adopted in this study; for a different target rotation angle, the same wheelbase would not necessarily correspond to an integer pulse count, and the general angular resolution of approximately $2\Delta s/L \approx 2.0$◦ per encoder count that accounts for both wheels rotating in opposite directions during a turn would then apply as the governing precision bound.

The controller drives both motors at a fixed target velocity in opposite directions and monitors θ in real time; once θ reaches the target value of 20◦ (converted to radians), the motors are stopped and the controller transitions back to the IDLE state. Encoder pulse counts are reset to zero at the start of each turning maneuver, since the system executes discrete incremental steps rather than tracking continuous heading over time.

F. Safety Mechanisms

Because classification uncertainty and transient EEG artifacts are inherent limitations of brain– computer interface systems, a multi-layered safety strategy was implemented to minimize unintended wheelchair motion. Safety measures are incorporated at both the software and embedded control levels to ensure that only reliable commands are executed while limiting the consequences of incorrect or delayed predictions.

a) **Software-Level Safety**: Before a command is transmitted to the embedded controller, the classifier output passes through a confidence-based validation stage. For each 1s analysis window, the classifier produces posterior probabilities for the four motor-imagery classes. A command is transmitted only when the maximum prediction confidence exceeds a predefined threshold; otherwise, the prediction is rejected and no control command is issued. The specific threshold value was determined empirically, as described in Section III. This confidence-based rejection strategy, commonly referred to in the literature as classification with a reject option, suppresses uncertain classifications and reduces the likelihood of unwanted wheelchair movements caused by noisy EEG signals [25].

b**) Embedded-Level Safety**: After receiving a validated command, several additional safety mechanisms govern the execution of the motion:

1) **Communication Timeout Watchdog**: Continuous forward motion represents the highest operational risk because, unlike the incremental steering states, it has no inherent completion condition. If no new validated command is received within 2s while the wheelchair is in the FORWARD state, the watchdog timer automatically stops both motors and forces a transition to the IDLE state.

2) **Self-Terminating Incremental Steering**: The LEFT and RIGHT states execute encoder based incremental rotations of approximately 20◦ before automatically returning to the IDLE state (Section II-E). This incremental steering strategy further reduces unintended continuous turning caused by transient EEG misclassifications while improving directional controllability.

3) **Transition Braking**: Direct transitions between active motion states are prohibited. Whenever a change of motion state is requested, the controller first decelerates the wheelchair to a complete stop before initiating the next movement. This strategy reduces mechanical stress and prevents abrupt changes in direction (Section II-E).

4) **Hardware Emergency Cutoff**: A physical emergency-stop switch is connected directly to the enable lines of the L298N motor driver, providing an independent hardware level shutdown mechanism. Activating the switch immediately removes power from both drive motors regardless of the controller state or software execution.

III. EXPERIMENTAL RESULTS

A**. Classifier Comparison Using Cross-Validation**

To identify the most suitable classifier for the proposed EEG-based wheelchair control system, three supervised machine learning algorithms, namely Support Vector Machine (SVM), k-Nearest Neighbors (KNN), and Linear Discriminant Analysis (LDA), were evaluated using five-fold stratified cross-validation. Classification performance was assessed using both classification accuracy and Cohen's Kappa coefficient to measure predictive performance and agreement beyond chance.

Table II summarizes the classification accuracy obtained for each fold together with the mean and standard deviation, while Table III reports the corresponding Cohen's Kappa values.

TABLE II. FIVE-FOLD CROSS-VALIDATION ACCURACY (%)

Fold	SVM	KNN	LDA
Fold 1	90.7	90.7	88.9
Fold 2	87.0	87.0	81.5
Fold 3	88.9	90.7	87.0
Fold 4	92.6	87.0	87.0
Fold 5	94.4	88.9	85.2
Mean ± SD	90.7 ± 2.6	88.9 ± 1.7	85.9 ± 2.5

TABLE III: FIVE-FOLD CROSS-VALIDATION COHEN'S KAPPA

Fold	SVM	KNN	LDA
Fold 1	0.876	0.876	0.852
Fold 2	0.827	0.827	0.753
Fold 3	0.852	0.876	0.827
Fold 4	0.901	0.827	0.827
Fold 5	0.926	0.852	0.802
Mean ± SD	0.876 ± 0.035	0.852 ± 0.022	0.812 ± 0.033

As shown in Tables II and III, the SVM classifier achieved the highest mean performance across the five cross-validation folds, yielding a mean classification accuracy of 90.7 ± 2.6% and a mean Cohen's Kappa of 0.876 ± 0.035, outperforming the other classifiers on three of the five folds and tying with KNN on one-fold. KNN exhibited competitive performance with an average accuracy of 88.9 ± 1.7%, whereas LDA produced the lowest overall performance with a mean accuracy of 85.9 ± 2.5% and the lowest mean Kappa value of 0.812±0.033. The higher Kappa value obtained by SVM further indicates stronger agreement between the predicted and true class labels beyond chance. Based on these results, SVM was selected as the classification model for the subsequent hardware in-the-loop (HIL) evaluation.

To further examine the class-wise distribution of correct classifications and misclassifications, the confusion matrices obtained from the cross validation predictions are presented in Fig. 5. The matrices illustrate the distribution of correct classifications and misclassifications for each classifier.

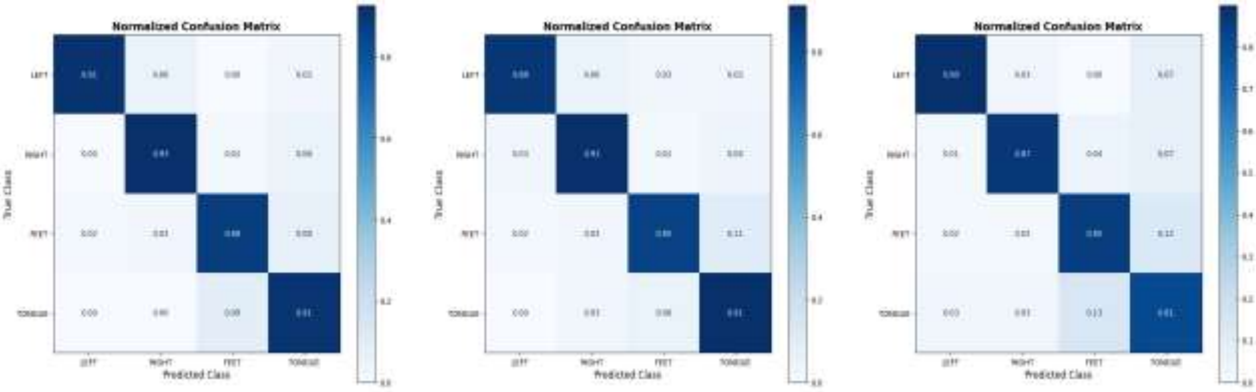

(a) SVM **(b) KNN** **(c) LDA**

FIGURE 5. **Confusion matrices of the evaluated classifiers.**

The confusion matrices further support the quantitative results reported in Tables II and III. The SVM classifier exhibits the strongest diagonal dominance, indicating the highest proportion of correctly classified motor imagery trials and the fewest inter-class confusions. KNN demonstrates comparable performance with slightly increased confusion among similar classes, whereas LDA produces the largest number of misclassifications, particularly for the Feet and Tongue classes. These observations further support the selection of SVM for the subsequent hardware-in-the-loop evaluation.

B. **Hardware-in-the-Loop (HIL) Evaluation**

Following classifier selection through cross validation, the SVM model was further evaluated using a Hardware-in-the-Loop (HIL) replay experiment to assess the practical performance of the proposed EEG-based wheelchair control framework. The unseen dataset, which was not used during model training or cross-validation, was replayed sequentially to emulate wheelchair operation under realistic sequential control conditions.

The HIL framework employs an offline replay based emulation of a real-time control loop, in which pre-recorded, discrete EEG trials from the independent holdout set each spanning the fixed 0.5– 3.5s analysis window established in Section II-A are processed sequentially by the trained FBCSP–SVM classifier. Trials are replayed at a fixed pacing interval of 1s, emulating the cadence of a continuously operating system. The selected SVM classifier achieved an overall classification accuracy of 85.9% and a Cohen's Kappa coefficient of 0.812 on the unseen dataset during the HIL replay experiment. Figure 6 presents the corresponding confusion matrix, illustrating the distribution of correct classifications and misclassifications across the four motor imagery classes. The confusion matrix confirms that the classifier preserves good class discrimination on previously unseen dataset, with most samples correctly classified along the main diagonal.

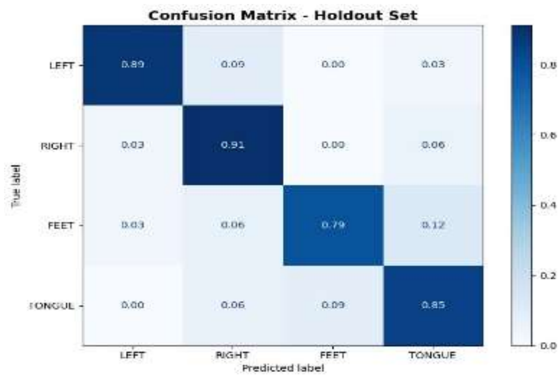

FIGURE 6. **Confusion matrix of the SVM classifier on unseen dataset.**

To further improve operational reliability, a confidence-based validation strategy was incorporated before transmitting commands to the embedded controller, accepting only predictions with a confidence score of at least 0.7. The threshold was empirically set to 0.7, as it approximately matches the average prediction confidence obtained during the HIL evaluation. At this operating point, the system achieves a favorable trade-off between command coverage and classification reliability, preserving 60.7% of the predictions while increasing the overall accuracy to 97.6%. Table IV summarizes the classification performance with and without confidence-based filtering, including overall and per-class accuracy.

TABLE IV. HIL CLASSIFICATION PERFORMANCE WITH AND WITHOUT CONFIDENCE-BASED FILTERING (τ = 0.7).

Metric	All Predictions	Confidence ≥0.7
Accuracy	85.9%	97.6%
Coverage	100%	60.7%
Errors	19	2
LEFT	88.6%	100%
RIGHT	91.2%	96.3%
FEET	78.8%	94.7%
TONGUE	84.8%	100%

Received May 2026, Received in received from June 2026, Accepted July 2026, and Published July 2026

Confidence-based filtering effectively suppresses uncertain predictions, reducing the error count from 19 to 2 while retaining 60.7% of the original predictions. The practical implications of this accuracy– coverage trade-off, together with the per-class differences observed in Table IV, are discussed in further detail in Section IV.

Overall, the HIL replay experiment demonstrates that the proposed EEG-based wheelchair control framework maintains stable classification performance on previously unseen dataset while providing reliable sequential command generation under pseudo-real-time operating conditions.

IV. DISCUSSION

The experimental results presented in Section III demonstrate that the proposed FBCSP–SVM pipeline, combined with confidence-based command validation and encoder-verified embedded motion control, constitutes a viable framework for EEG based wheelchair control. This section interprets these findings in relation to the overall system design and critically examines the limitations of the present study.

A. **Classifier Selection**

The cross-validation comparison indicated that SVM achieved the highest mean accuracy (90.7 ± 2.6%) and Cohen's Kappa (0.876±0.035) among the three evaluated classifiers, outperforming KNN and LDA on the majority of folds. This finding is consistent with the broader motor-imagery BCI literature, in which the nonlinear decision boundary afforded by the RBF kernel is often better suited to the overlapping class distributions typical of FBCSP feature spaces than the strictly linear boundary produced by LDA. LDA's comparatively lower performance may reflect its underlying assumption of a shared covariance structure across classes, which may not hold precisely across all four motor imagery tasks. The marginally lower performance of KNN, relative to SVM, is plausibly attributable to its sensitivity to local feature-space density, which can be affected by the moderate dimensionality of the 80-feature representation retained after feature selection.

B. **Generalization to Unseen Dataset**

The reduction in accuracy observed between cross-validation (90.7%) and the unseen dataset evaluation (85.9%) is both expected and methodologically reassuring. Cross-validation provides an estimate of generalization performance on the working dataset used for model development. Because hyperparameter optimization was performed using this same dataset, the resulting cross-validation accuracy may still represent a slightly optimistic estimate of performance. The independent holdout set, which remained completely isolated from both training and model selection, therefore provides a more realistic assessment of the classifier's ability to generalize to unseen trials.

C**. Effect of Confidence-Based Filtering**

The confidence-based validation stage exerted a substantial effect on system reliability. Restricting command execution to predictions with confidence ≥ 0.7 reduced the number of misclassified trials from 19 to 2, raising accuracy among accepted predictions to 97.6%, at the cost of rejecting approximately 39% of predictions and retaining 60.7% coverage. This accuracy coverage trade-off is a deliberate and, for a physically actuated system, an appropriate one: an erroneous command that produces unintended motion carries substantially greater consequence than a withheld command, given the residual, non-zero misclassification risk inherent to EEG decoding. The reduced coverage implies that a user may occasionally need to sustain a given motor imagery task across more than one prediction cycle before a command is accepted; this is judged a reasonable usability cost relative to the reliability gained.

The per-class results reported in Table IV indicate that this benefit is not uniformly distributed across classes. The FEET class exhibited the lowest accuracy both before (78.8%) and after (94.7%) filtering, whereas LEFT and TONGUE reached 100% accuracy among high-confidence predictions. This pattern is consistent with prior motor-imagery findings, in which imagined feet and tongue movements can elicit partially overlapping sensorimotor activation relative to the more laterally distinct left- and righthand imagery, occasionally resulting in greater interclass confusion.

D**. Limitations**

Several limitations of the present study warrant acknowledgment. First, the system was developed and evaluated using data from a single subject, following a subject-dependent classification paradigm; performance may differ substantially for other users, and subject-independent generalization was not assessed. Second, evaluation was conducted entirely offline: no live EEG acquisition was performed at any stage, and the HIL experiment relied on the sequential replay of pre-recorded, previously classified trials rather than a continuously operating live classification pipeline. Consequently, factors that would only manifest under live operating conditions including electrode impedance drift, Realtime artifact contamination, and user fatigue over extended sessions were not captured by the present evaluation. Third, the confidence threshold ($\tau = 0.7$) was selected on the basis of reasoned design tradeoffs rather than systematic optimization or user studies, and their suitability for real users operating the physical prototype has not been empirically validated. Finally, the steering increment (20°) was selected as a compromise between angular control accuracy and motion stability. While this relatively small increment enables more precise adjustment of the wheelchair orientation, larger rotation angles require multiple consecutive commands, which increases the time required to complete the maneuver.

Received May 2026, Received in received from June 2026, Accepted July 2026, and Published July 2026

V. CONCLUSION AND FUTURE WORK

This thesis presented the design, implementation, and evaluation of an EEG-based motor imagery brain–computer interface for wheelchair control, integrating an FBCSP feature extraction pipeline, a comparative evaluation of SVM, LDA, and KNN classifiers, and a physical wheelchair prototype governed by an encoder-based embedded control architecture. The SVM classifier, selected on the basis of five-fold stratified cross-validation, achieved a mean accuracy of 90.7% and a Cohen's Kappa of 0.876, and subsequently attained 85.9% accuracy on an unseen dataset under Hardware-in-the-Loop evaluation. The introduction of confidence-based command validation substantially improved command reliability, increasing the accuracy of accepted predictions to 97.6% while maintaining a command coverage of 60.7%. To enhance operational safety, the embedded control architecture incorporated a multi-tiered safety strategy comprising confidence gating, self-terminating steering, transition braking, communication timeout supervision, and a hardware emergency cutoff to mitigate the effects of residual classification uncertainty. Collectively, these results demonstrate that the integration of accurate motor imagery classification, confidence-based command validation, and a layered embedded safety architecture provide a robust and practical framework for EEG-based wheelchair control despite the inherent uncertainty of EEG-based decoding.

Several directions for future work follow directly from the limitations identified in Section IV. Foremost among these is the extension of the present offline framework to live, closed-loop operation, incorporating real-time EEG acquisition and signal processing in place of the replay-based HIL methodology employed in this study. Evaluation across multiple subjects would further establish whether the reported performance generalizes beyond the single-subject, subject-dependent paradigm adopted here, and would inform the feasibility of a subject independent or rapidly calibrated variant of the system.

An important direction for future work is the comparative evaluation of deep learning architectures, such as convolutional neural networks purpose-built for EEG decoding (e.g., EEG Net or similar compact architectures), against the FBCSP based pipeline employed here. While such architectures have demonstrated strong performance in recent motor-imagery BCI literature, they typically require larger training datasets and impose greater computational demands.

Empirical tuning of the confidence threshold and steering increment, informed by trials with real users rather than design assumptions alone, would help establish operating parameters that balance responsiveness and safety more precisely than the values adopted in this study. Finally, given the comparatively weaker classification performance observed for the FEET class, the investigation of class specific confidence thresholds or additional feature engineering targeted at improving feet/tongue discriminability represents a promising avenue for enhancing the overall balance and reliability of the proposed control framework.

REFERENCES

[1] M. Rashid, N. Sulaiman, A. PP Abdul Majeed, R. M. Musa, A. F. Ab. Nasir, B. S. Bari, and S. Khatun, "Current status, challenges, and possible solutions of EEG-based brain-computer interface: a comprehensive review," *Frontiers in neurorobotics*, vol. 14, p. 25, 2020.

[2] A. Palumbo, V. Gramigna, B. Calabrese, and N. Ielpo, "Motorimagery EEG-based BCIs in wheelchair movement and control: A systematic literature review," *Sensors*, vol. 21, no. 18, p. 6285, 2021.

[3] A. Saibene, M. Caglioni, S. Corchs, and F. Gasparini, "EEGbased BCIs on motor imagery paradigm using wearable technologies: a systematic review," *Sensors*, vol. 23, no. 5, p. 2798, 2023.

[4] C. Brunner, R. Leeb, G. Muller-Putz,¨ A. Schlogl,¨ and G. Pfurtscheller, "BCI competition 2008–graz data set a," *Institute for knowledge discovery (laboratory of brain-computer interfaces), Graz University of Technology*, vol. 16, no. 1-6, p. 1, 2008.

[5] Abdullah, I. Faye, and M. R. Islam, "EEG channel selection techniques in motor imagery applications: A review and new perspectives," *Bioengineering*, vol. 9, no. 12, p. 726, 2022.

[6] Z. Ma, K. Wang, M. Xu, W. Yi, F. Xu, and D. Ming, "Transformed common spatial pattern for motor imagery-based brain-computer interfaces," *Frontiers in neuroscience*, vol. 17, p. 1116721, 2023.

[7] E. Dagdevir and M. Tokmakci, "Optimization of preprocessing stage in EEG based BCI systems in terms of accuracy and timing cost," *Biomedical Signal Processing and Control*, vol. 67, p. 102548, 2021.

[8] K. K. Ang, Z. Y. Chin, H. Zhang, and C. Guan, "Filter bank common spatial pattern FBCSP in brain-computer interface," in *2008 IEEE international joint conference on neural networks (IEEE world congress on computational intelligence)*. IEEE, 2008, pp. 2390–2397.

[9] F. Lotte, L. Bougrain, A. Cichocki, M. Clerc, M. Congedo, A. Rakotomamonjy, and F. Yger, "A review of classification algorithms for EEG-based brain–computer interfaces: a 10 year update," *Journal of neural engineering*, vol. 15, no. 3, p. 031005, 2018.

[10] C. Zhang and A. Eskandarian, "A computationally efficient multiclass time-frequency common spatial pattern analysis on EEG motor imagery," in *2020 42nd Annual International Conference of the IEEE Engineering in Medicine & Biology Society EMBC*. IEEE, 2020, pp. 514–518.

[11] J. Dong, M. Komosar, J. Vorwerk, D. Baumgarten, and J. Haueisen, "Scatter-based common spatial patterns–a unified spatial filtering framework," *arXiv preprint arXiv:2303.06019*, 2023.

[12] B. Gu, M. Xu, L. Xu, L. Chen, Y. Ke, K. Wang, J. Tang, and D. Ming, "Optimization of task allocation for collaborative brain–computer interface based on motor imagery," *Frontiers in Neuroscience*, vol. 15, p. 683784, 2021.

[13] X. Xiong, Y. Wang, T. Song, J. Huang, and G. Kang, "Improved motor imagery classification using adaptive spatial filters based on particle swarm optimization algorithm," *Frontiers in Neuroscience*, vol. 17, p. 1303648, 2023.

[14] S. Kumar, A. Sharma, and T. Tsunoda, "An improved discriminative filter bank selection approach for motor imagery EEG signal classification using mutual information," *BMC bioinformatics*, vol. 18, no. Suppl 16, p. 545, 2017.

[15] J. Luo, X. Gao, X. Zhu, B. Wang, N. Lu, and J. Wang, "Motor imagery EEG classification based on ensemble support vector learning," *Computer methods and programs in biomedicine*, vol. 193, p. 105464, 2020.

[16] J. Ma, B. Yang, W. Qiu, Y. Li, S. Gao, and X. Xia, "A large EEG dataset for studying cross-session variability in motor imagery brain-computer interface," *Scientific Data*, vol. 9, no. 1, p. 531, 2022.

[17] C. Cortes and V. Vapnik, "Support-vector networks," *Machine learning*, vol. 20, no. 3, pp. 273–297, 1995.

[18] J. Jiang, C. Wang, J. Wu, W. Qin, M. Xu, and E. Yin, "Temporal combination pattern optimization based on feature selection method for motor imagery BCIs," *Frontiers in Human Neuroscience*, vol. 14, p. 231, 2020.

[19] C.-C. Chang and C.-J. Lin, "LIBSVM: A library for support vector machines," *ACM transactions on intelligent systems and technology (TIST)*, vol. 2, no. 3, pp. 1–27, 2011.

[20] A. Geron,´ *Hands-on machine learning with Scikit-Learn, Keras, and TensorFlow*. " O'Reilly Media, Inc.", 2022.

[21] M. Rashid, B. S. Bari, M. J. Hasan, M. A. M. Razman, R. M. Musa, A. F. Ab Nasir, and A. P. A. Majeed, "The classification of motor imagery response: an accuracy enhancement through the ensemble of random subspace k-NN," *PeerJ Computer Science*, vol. 7, p. e374, 2021.

[22] T. Hastie, R. Tibshirani, J. Friedman *et al.*, "The elements of statistical learning," 2009.

[23] E. Mohammadi, P. G. Daneshmand, and S. M. S. M. Khorzooghi, "Electroencephalography-based brain–computer interface motor imagery classification," *Journal of Medical Signals & Sensors*, vol. 12, no. 1, pp. 40–47, 2022.

[24] M. Ferreira, L. Moreira, and A. Lopes, "Differential drive kinematics and odometry for a mobile robot using TwinCAT." *Electronic Research Archive*, vol. 31, no. 4, 2023.

[25] D. Milanes-Hermosilla, R. Trujillo-Codorniu, S. LamarCarbonell, R. Sagaro-Zamora, J. J. Tamayo-Pacheco, J. J. Villarejo-Mayor, and D. Delisle-Rodriguez, "Robust motor imagery tasks classification approach using bayesian neural network," *Sensors*, vol. 23, no. 2, p. 703, 2023.